Dryout and Power Distribution Effects in Boiling Water Reactors

by

Carl Adamsson

October 2009
Technical Reports from
AlbaNova University Center
Royal Institute of Technology
Nuclear Reactor Technology
SE-106 91 Stockholm, Sweden

Akademisk avhandling som med tillstånd av Kungliga Tekniska Högskolan i Stockholm framlägges till offentlig granskning för avläggande av teknologie doktorexamen fredagen den 13 November 2009 kl 10.15 i sal FR4, AlbaNova Universitetscentrum, Roslagtullsbacken 21, Stockholm.

Universitetsservice US–AB, Stockholm 2009

Carl Adamsson 2009, **Dryout and Power Distribution Effects in Boiling Water Reactors**

AlbaNova University Center, Nuclear Reactor Technology, SE-106 91 Stockholm, Sweden

Abstract

Film flow measurements at several axial positions in round pipes with various axial power distributions are presented for conditions corresponding to normal operation of a BWR. It is confirmed that the film flow rate approaches zero at the onset of dryout. Selected phenomenological models of annular two-phase flow are shown to reasonably reproduce the measurements. It is concluded that models are in better agreement with measurements if terms corresponding to possible boiling induced entrainment are excluded.

A method to perform film flow analysis in subchannels as a post-process to a standard two-field subchannel code is suggested. It is shown that this approach may yield accurate prediction of dryout power in rod bundles to a low computational cost and that the influence of the power distribution is well predicted by the model.

Descriptors: Dryout, Film flow analysis, Power distribution, Measurements, Subchannel

Preface

This thesis consists of two parts. The first is an introduction and summary of the present work that provides some background and overview as well as summarizes the main results and conclusions. The second part consists of five published papers, which have been adjusted to comply with the format of the thesis, but have not been changed except for minor refinements.

August 2009, Stockholm
Carl Adamsson

Some like to understand what they believe in.
Others like to believe in what they understand.
—Stanislaw Jerzy Lec

List of Publications

Papers Included in the Thesis

Paper 1

Measurements of the Liquid Film Flow Rate in High Pressure Annular Flow with Various Axial Power Distributions

C. Adamsson and H. Anglart

Published at *HEAT 2005, Gdansk, Poland, June 26–30, 2005*

Paper 2

Eperimental Investigation of the Liquid Film for Annular Flow in a Tube with Various Axial Power Distributions

C. Adamsson and H. Anglart

Published at *NURETH 11, Avignon, France, October 2–6, 2005*

Paper 3

Film Flow Measurements for High Pressure Diabatic Annular Flow in Tubes with Various Axial Power Distributions

C. Adamsson and H. Anglart

Published in *Nuclear Engineering and Design 236(23), 2006, Pages 2485–2493*

Paper 4

Modeling and Validation of a Mechanistic Tool (MEFISTO) for the Prediction of Critical Power in BWR Fuel Assemblies

J.M. Le Corre and C. Adamsson

Submitted to *Nuclear Engineering and Design*

Paper 5

Influence of Axial Power Distribution on Dryout: Film-Flow Models and Experiments

C. Adamsson and H. Anglart

Submitted to *Nuclear Engineering and Design*

Papers not Included

A Reinterpretation of Measurements in Developing Annular Two-Phase Flow

C. Adammsson and H. Anglart at *The 13th Internation Topical Meeting on Nuclear Reactor Thermal Hydraulics (NURETH-13)*, Kanazawa City, Ishikawa Prefecture, September 27–October 2, 2009

An Assessment of Entrainment Correlations for the Dryout Prediction in BWR Fuel Bundles

F. Secondi, C. Adamsson and J.M. Le Corre *The 13th Internation Topical Meeting on Nuclear Reactor Thermal Hydraulics (NURETH-13)*, Kanazawa City, Ishikawa Prefecture, September 27–October 2, 2009

A Sensitivity Study of Lagrangian Models for Application to Annular Two-Phase Flows

C. Adamsson and H. Anglart at *Nuclear Energy for New Europe*, Portoroz, Slovenia, September 10–13, 2007

An Investigation of Cross-Section Geometry Effects on the Deposition Rate in Annular Two-Phase Flows with a Lagrangian Model

C. Adamsson and H. Anglart at *The 12th Internation Topical Meeting on Nuclear Reactor Thermal Hydraulics (NURETH-12)*, Pittsburgh, Pennsylvania, U.S.A. September 30–October 4, 2007

The Mona Subchannel Analysis Code — Part B: Validation and Verification

C. Adamsson, H. Anglart, M. Nordsveen and N. Hoyer at *The 10th Internation Topical Meeting on Nuclear Reactor Thermal Hydraulics (NURETH-10)*, Seoul, Korea, October 5–9, 2003

The Mona Subchannel Analysis Code — Part A: Model Description

M. Nordsveen, N. Hoyer, C. Adamsson and H. Anglart, at *The 10th Internation Topical Meeting on Nuclear Reactor Thermal Hydraulics (NURETH-10)*, Seoul, Korea, October 5–9, 2003

Contents

Part I

Overview and summary

CHAPTER 1

Background

The story about nuclear reactors has two sides. One is that of the atomic nucleus, the magnificent amount of energy that can be released by splitting them and how physicists have learned to master a self-sustained, stable and controllable chain reaction. The other is the story about how all that energy makes it safely out of the reactor vessel. This question belongs to the field of thermal-hydraulics, dating back, not to the Manhattan project, but to the industrial revolution and the development of the steam engine.

The vast majority of electricity producing nuclear reactors currently operating in the world are cooled by light water flowing in vertical channels through the reactor core. This process always has to be efficient enough to prevent the fuel from reaching temperatures, which can cause damage to the core. It is thus of great importance to be able to predict the value of the heat transfer coefficient under all possible conditions that may occur in the reactor during normal operation as well as during various abnormal or accident conditions.

The heat transfer coefficient is, in general, a complex function of channel geometry, heater surface properties, flow conditions and properties of the coolant. The possibility of boiling in the coolant adds another layer of complexity since the generation of vapor will significantly influence the flow pattern and hence the heat transfer rate. Boiling is, however, normally a very efficient heat transfer mechanism that is deliberately utilized in the boiling water reactor (BWR) design. In pressurized water reactors (PWR) there is no boiling in the bulk of the coolant flow but local, so called sub-cooled boiling, normally occurs. Boiling of the coolant is hence a reality in practically all existing nuclear reactor designs.

Even though boiling heat transfer usually is efficient in removing heat from the fuel there is a limit at high enough heat flux where the heat transfer coefficient is suddenly and drastically reduced. This point is usually called the critical heat flux (CHF) or the boiling crisis. At higher heat fluxes the heater temperature increases greatly to levels where fuel damage may occur in a reactor. The reactor power thus has to be limited so that sufficient margin to CHF is guaranteed at any time and any location in the core. On the other hand there is always a commercial interest to extract as much power as possible from the

reactor. It follows that there is a great interest to predict the onset of CHF as accurately as possible and to find methods to increase the critical power level.

Naturally the CHF phenomenon has been subject to a great deal of experimental as well as theoretical research. The phenomenon has, however, turned out to be utterly complex and it is probably fair to say that many details are still not properly understood. In fact, when the mechanisms are studied more closely the CHF phenomenon branches up in several related phenomena depending on the flow conditions. Hence, the type CHF that occurs in the usually bubbly flow regime of a PWR is termed departure from nucleate boiling (DNB) whereas the CHF mechanism in the annular flow regime of a BWR is called dryout. (Alternative terminology, such as burnout, boiling transition etc., is sometimes used. The exact definitions of these concepts may vary from author to author, but this text will stick to definitions above, which are the most common in recent literature).

It should be noted that the fuel temperature is not monitored in the reactor during operation. The thermal margins thus depend entirely on the heat transfer models that are used in various safety analysis and core monitoring computer codes. In order to assure that thermal limitations are never exceeded such codes always have to account for the uncertainty in the models and increase margins accordingly to be on the safe side. It follows that improved accuracy of the models, in itself, would allow increased reactor power without any modification to the fuel or reactor while preserving the safety margins.

Accurate models also give the opportunity to optimize the fuel design and the operation of the reactor in various ways. This may involve modifications of the geometrical structure of the fuel assemblies but also techniques that are routinely applied in the operation of reactors, such as movements of control rods and careful fuel design with various enrichments and burnable absorbers. These techniques have in common that they manipulate the distribution of power in the reactor, which has turned out to confuse many commonly used dryout models. This issue and in particular the axial power distribution is the main topic of the present thesis. The scope is limited to BWR applications and the dryout phenomenon.

Chapter 2 discusses the dryout phenomenon from a phenomenological as well as a mechanistic perspective. The physical mechanisms that govern the onset of dryout are rather well understood, at least in a qualitative sense. The need for detailed and quantitative measurements is still great, however. The techniques of film flow measurements are treated in Chapter 3 and a set of new measurements are presented that will add to and confirm the present understanding of the dryout phenomenon.

The standard tools for prediction of dryout margins are currently empirical correlations, which require large experimental studies and do not handle complex power distributions well. The interest in mechanistically based models is

therefore great but they have not yet been able to satisfy the requirements on accuracy and computational performance. These issues are discussed in Chapter 4, which gives an overview of traditional correlation techniques and treat film flow models in some more detail.

In order for film flow analysis to be applicable to the complex geometry of a real fuel bundle it has to be combined with subchannel analysis. This methodology is discussed in Chapter 5 and a partly novel method is introduced that dramatically cuts computational time while providing an accuracy comparable to fine-tuned empirical correlations. This model is evaluated in Papers 4–5 and is shown to correctly predict the influence of complex power distributions.

CHAPTER 2

The Dryout Phenomenon

In order to comprehend the various models and correlation attempts as well as a certain amount of confusion in terminology it may be helpful to consider separately the effects of dryout and how it has been traditionally measured on the one hand and the mechanisms that cause these effects on the other hand. We may refer to these views respectively as the parametric view and microscopic, or mechanistic, view. This chapter will treat the microscopic view first and then discuss the parametric trends, which, by this anachronistic outline, can be treated in the light of the mechanistic results. At the end of the chapter the two views are compared in a discussion of the main subject of this thesis: the influence of the axial power distribution.

2.1. Mechanisms of film dryout

In a BWR under normal operating conditions the flow regime in the upper part of the core will be annular, i.e. the vapor phase will occupy most of the volume and the liquid water will travel partly as a film attached to the walls and partly as drops entrained in the vapor stream. The fuel rods are cooled by evaporation of the liquid film flowing on the rod surface. A large amount of work, over several decades, has been spent on understanding the transition from this mode of efficient heat transfer to dryout. Today the fundamental mechanisms are, at least qualitatively, well understood. It is generally agreed upon that dryout occurs when the liquid film is no longer able to efficiently wet the wall so that heat, instead of evaporating the film, must be transported away from the wall by forced convection to the vapor phase and evaporation of liquid drops that deposit on the surface.

This section is thus largely concerned with the dynamics of the liquid film and the mechanisms that may cause its disappearance. Essentially the process can be described as a competition between mechanisms that drain the film of liquid and mechanisms rebuilding it.

2.1.1. *Deposition*

The entrained drops have their own dynamics as they follow the vapor stream in the core of the channel. As they collide with the liquid film at the wall they may deposit and build up the film. The rate of deposition may be measured

by the film extraction technique described in Chapter 3 applied in two subsequent positions (e.g. Okawa *et al.* (2005)). Another technique to measure the deposition rate is to study the development of a tracer liquid inserted into the film (Schadel *et al.* 1990).

A relatively large amount of measurement data of the deposition rate is available, but the details of the deposition mechanism are not completely understood. It is commonly assumed that drops deposit by a mechanism of turbulent dispersion but it seems likely that a mechanism of direct impaction contributes as well (Azzopardi 1987), (Azzopardi 1997). It is also interesting that the deposition rate seems to be almost independent of the gas flow rate (Schadel *et al.* 1990). This is not the expected behavior if the gas phase turbulence were driving the deposition process.

Another indication that turbulence has a rather small effect on the deposition rate comes from the experimental and computational study by Govan *et al.* (1989). Based on detailed measurements of the motion of small glass spheres in a turbulent gas stream they concluded that the injection method and the lateral lift force are more important than the gas turbulence.

Another issue, with direct implication for reactor applications, is that measurements of deposition in steam-water mixtures at 7 MPa pressure show an order of magnitude less deposition than measurements at atmospheric conditions. This trend does not seem to have been explained (Caraghiaur *et al.* 2009).

Despite this lack of understanding as to the details of the deposition mechanism the amount of experimental data at various conditions makes it possible to construct reasonably reliable correlations for the deposition rate. This is further discussed in Chapter 4.

2.1.2. *Film entrainment*

Liquid film flowing on a heated wall is depleted by evaporation. This process is, however, easily modeled (Chapter 4) and therefore not further discussed here. Much more complex is a process that is usually referred to as entrainment, whereby film is being sheared off the surface by the high velocity vapor stream. It has been shown photographically (Whalley *et al.* 1979) that this type of entrainment occurs by undercutting and break-up of large roll waves on the film surface. This process is illustrated in Fig. 2.1.

No direct measurements of the entrainment rate seem to exist. It may, however, be indirectly studied by measurements of the liquid film flow. If these are corrected for the rate of deposition, based on available empirical correlations, the entrainment rate remains.

It is somewhat unclear whether the heat flux causes additional entrainment by vapor bubbles bursting through the film, possibly carrying some liquid into the vapor stream. It has been argued that the rate of entrainment depends

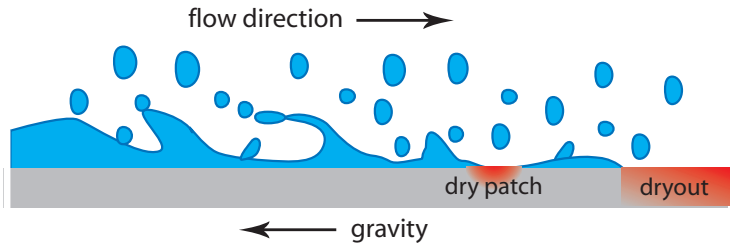

FIGURE 2.1. Idealized picture of annular flow close to a heated wall.

strongly on the heat flux (Milashenko *et al.* 1989). For falling liquid films the existence of boiling entrainment was demonstrated experimentally by Ueda & Isayama (1981) but it is not clear whether this has any significance for the conditions considered here. It seems probable that answer depends on the flow conditions; a thick liquid film and high heat flux is probably more likely to generate entrainment due to boiling. It is argued in Paper 2 of this thesis that boiling entrainment is probably not particularly important at typical BWR operating conditions.

2.1.3. *Critical film thickness*

The wavy structure of the film (Fig. 2.1) makes it more difficult to define exactly when the film has dried out. When the film is thin dry patches may form on the heater surface for a short time before being rewetted by the next wave. This is observed as oscillations of the heater temperature just prior to dryout.

A related issue is whether the film thickness will go continuously to zero as the dryout power is approached or if there is a critical film thickness where the film, for one reason or another, will suddenly break up and dryout occur. Experiments by Milashenko *et al.* (1989) and Ueda & Isayama (1981) indicate significant critical film thickness, while experiments by Hewitt *et al.* (1965) and, as will be shown, the present experiments (Paper 1–3) imply that it is negligible. This discrepancy is most likely due to the fact that the first two experiments, which showed critical film, were performed in much shorter tubes (around 1 m) and correspondingly higher heat fluxes than the latter (3–4 m).

2.2. A parametric view of dryout

Measurements of dryout power are typically performed in thermal hydraulic test loops where the coolant passes through and boils in an electrically heated test-section. It is then circulated through a condenser and a pre-heater, which controls the temperature at the inlet of the test-section. Usually the coolant mass flow-rate, the outlet pressure and the inlet temperature are fixed while the power is increased slowly until dryout occurs. The dryout is detected by

monitoring the wall temperature of the heater; a characteristic temperature excursion indicates that a dryout has occurred.

By this method it is possible to systematically build large databases that can be used as look-up tables for the dryout power. For round pipes an immense amount of accurate data is available for a wide range of conditions (Groeneveld *et al.* 2007). However, the dryout power is very sensitive to the geometry of the channel. It is thus rather difficult to make accurate predictions of the dryout power in realistic fuel bundles based on measurements in simple geometry. Instead fuel vendors perform their own dryout measurements in full scale mock-up fuel bundles (Helmersson *et al.* 2006) and typically use these to construct fuel specific correlations for the dryout power (Chapter 4).

When discussing paramteric trends it is, obviously, fundamental to define which the parameters are. In particular it has to be clear exactly which parameters are fixed as one parameter vary. Unfortunately, this has sometimes been more or less implicitly assumed, causing some confusion. Here, we will try to make it clear. The following independent parameters will be discussed: pipe length, coolant mass flow rate at the inlet, pressure at the outlet and inlet subcooling (in terms of temperature). For the dependent parameter there are several commonly used options: the dryout power, the dryout heat flux or the dryout steam quality. These three parameters all provide valuable information depending on the context. We will therefore, where so needed, discuss them in parallel.

The main parametric trends are discussed below. Even though the discussion is concerned with uniformly heated round tube, the information is qualitative and applies with minor adoptions also to rod bundles. For most part the description follows Hewitt in the book by Hetsroni (1982).

1. Tube length: The total dryout power and hence the outlet steam quality increases with tube length. The dryout heat flux, on the other hand, decreases with tube length. Some data show an asymptotically constant power/steam quality. This trend is easy to understand from the mechanistic perspective; if the pipe length were increased at constant power, the heat flux and hence evaporation rate would fall. Deposition, which always dominates over entrainment close to the dryout point, becomes relatively stronger and postpones the dryout. Note that it is not necessary to refer to e.g. boiling entrainment.
2. Subcooling: The dryout power increases approximately linearly with increasing subcooling. The steam quality, however, decreases. This parameter is closely related to the tube length. In fact, an arbitrarily long subcooled inlet could be added to the pipe without changing anything in the boiling part of the channel if the subcooling is adjusted to preserve the steam quality. This idea naturally leads to the boiling length parameter discussed in Section 4.1.

3. Pressure: As the pressure is increased from atmospheric conditions towards the critical point (beyond which the dryout phenomenon obviously does not exist in the form discussed here) the dryout power passes through a maximum. The exact location of the maximum varies depending on other parameters but it typically occurs between 3 MPa and 7 MPa. The steam quality passes through a maximum as well but it occurs at a slightly higher pressure. This trend is very complex since several important properties of water vary considerably with pressure. It is interesting to note the large and seemingly unexplained variation of the deposition rate with pressure (Section 2.1.1).
4. Mass flux: At low mass flux the dryout power increases rapidly with increasing mass flux to approach a constant value at high mass flux. The dryout quality decreases with increasing mass flux. This trend can be understood by considering that the entrainment rate increases considerably with increasing mass flux, whereas the deposition rate is almost constant. More entrained droplets at dryout means lower dryout quality.

There are, however, effects which are not easy to study parametrically, the most notorious probably being the axial power distribution (APD). There are two main reasons that this parameter is difficult: first it can obviously not be described by a single number and is hence difficult to systematically vary and tabulate. Second, it is, for technical reasons, very expensive to vary the APD in an electrically heated test section (one test section for each power distribution is usually necessary).

As was mentioned in Chapter 1 the distribution of power in a fuel assembly may vary significantly for a number of reasons. Measurements of dryout power has shown that the power distribution can have a great impact on the dryout power; i.e. at a fixed power level, dryout may or may not occur depending on the relative distribution of power within the assembly. As this is the main subject of the present thesis and the mechanistic explanation is somewhat complicated it is devoted a separate section below.

2.3. Influence of the axial power distribution

From available experimental investigation of the APD effect, e.g. (Becker *et al.* 1981) and (Blomstrand *et al.* 2000), it can be concluded that shifting power towards the outlet will decrease the dryout power, while shifting it towards the inlet will increase the power at which dryout occurs. This trend appears to be general but the magnitude of the effect depends on the channel geometry, location of possible spacer grids and on the particular shape of the power distribution (Paper 5).

A possible hypothesis would be that it is the local heat flux that governs the transition to dryout. High heat flux close to the channel outlet, where

the steam quality is high, would then act to reduce the total dryout power. However, experiments with a 'flux spike' — a very short axial segment with very high heat flux — have shown that at high steam quality the spike had almost no effect on the dryout power (Groeneveld 1975). Nevertheless, many dryout correlations are built on this hypothesis, as discussed in Section 4.1.

The real mechanism behind this effect is much more complex as was demonstrated in an elegant series of experiments by Bennett *et al.* (1966). They measured the dryout power and the axial variation of the film flow rate in a round pipe that was uniformly heated except for a moveable cold patch. The power could hence be continuously shifted between the inlet and the outlet without changing the local heat flux at the dryout point. It was observed that the dryout power increased when the cold patch was placed close to the outlet thus creating a bottom-shifted power distribution. Strikingly it was in this way possible to achieve a higher dryout power than with a completely uniform power distribution, even though the local heat flux had to be slightly higher (Fig. 2.2).

The mechanism is most readily explained by considering the flow rate of entrained droplets and how it evolves axially in the channel. This value is easily obtained by subtracting from the total flow rate the film flow, which was measured, and the vapor flow, calculated from the heat balance. Fig. 2.3 is reproduced from the original paper. It shows the flow rate of entrained drops versus the steam quality for different placements of the cold patch. It also shows the hydrodynamic equilibrium curve, i.e. the division film and droplets where deposition equals entrainment. This curve was obtained by measurements of fully developed adiabatic flow with various steam quality in very long pipes.

At the cold patches the entrained droplet curve tends towards the equilibrium curve. When the cold patch is close to the inlet this leads to an increased drop flow rate and thus a reduction in the dryout steam quality. When the cold patch is close to the outlet, on the other hand, the tendency towards equilibrium will reduce the amount of drops and increase the dryout steam quality. Dryout is here supposed to occur when the entrained drop curve meets the total liquid line, i.e. when the film flow rate is zero.

These experiments provide a clear mechanistic explanation of the observed APD effect as well as quantitative data that can be used to evaluate models. It is shown in Paper 5 that modern film flow models (Chapter 4) are able to reproduce these measurements. The cold patch power distributions, however, are extreme: ingeniously designed to study a specific phenomenon but not similar to anything that can be found in a reactor. Similar measurements of the axial film flow variation but with realistic power distributions at typical operating conditions of a BWR are presented in Papers 1–3 of this thesis. These experiments are further discussed in Chapter 3.

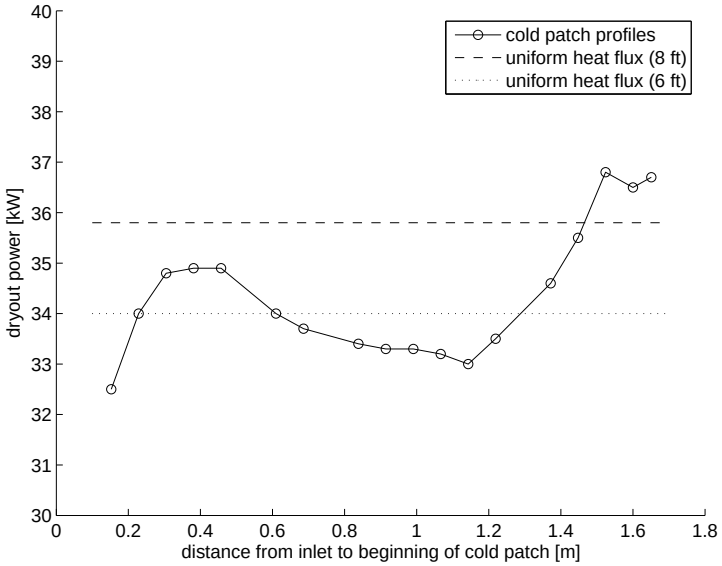

FIGURE 2.2. Experimental dryout power in 8 ft pipe with 2 ft cold patch (Bennett *et al.* 1966). Mass flux = 297 kg/m^{2}s and pressure = 0.38 MPa.

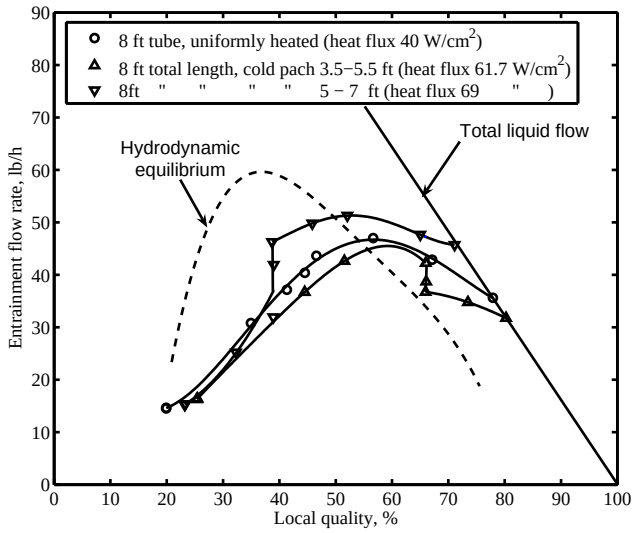

FIGURE 2.3. Reproduced from Bennett *et al.* (1966)

CHAPTER 3

Experimental Techniques

3.1. Earlier Experiments

Since dryout is triggered by the disappearance of the liquid film from the heated surface, the key to understanding the phenomenon is accurate measurements of the film. For this purpose one could measure either the thickness of the film or the film mass flow rate. The thickness has been measured with needle probes (Würtz 1978) and conductance probes (Collier & Hewitt 1964). These techniques are fast and make it possible to measure not only the average film thickness but also the waves traveling with the film. In dryout modeling, however, it is usually the mass flow rate that turns up in the equations, since this parameter can easily be related to the mass- and energy balances. For that reason it was decided to measure the film mass flow rate in this project.

A technique to do that by extracting the liquid film through the wall of the test-section has been shown to be reliable by several studies before. The idea is to slowly increase the extraction rate from a low value and at each step measure the amounts of liquid and gas in the sample. (In air-water systems this can be done with a separator, for steam-water systems the most reliable method is to condense the sample and rely on the heat balance as described below). When the flow of liquid no longer increases as the extraction rate is increased, it is assumed that the film flow rate has been found.

The earliest such experiments were performed on air-water systems and a slit in the wall was used to extract the film (Bennett & Thornton 1961). Since large waves in the film tend to overshoot the slit, it was replaced by a porous wall section in later studies. Hewitt *et al.* (1965) and Hewitt & Pulling (1969) used sinter metal wall sections and Würtz (1978) used a 5 cm wall section perforated with 1.2 mm holes. Singh *et al.* (1969) studied the influence of the length of the porous wall section and concluded that waves will overshoot if it is too short. On the other hand, if it is too long the measurements will be inaccurate. It was recommended to use a length of 1 in. In accordance with this recommendation, the present study used a 30 mm sinter metal wall section (with effective length slightly shorter).

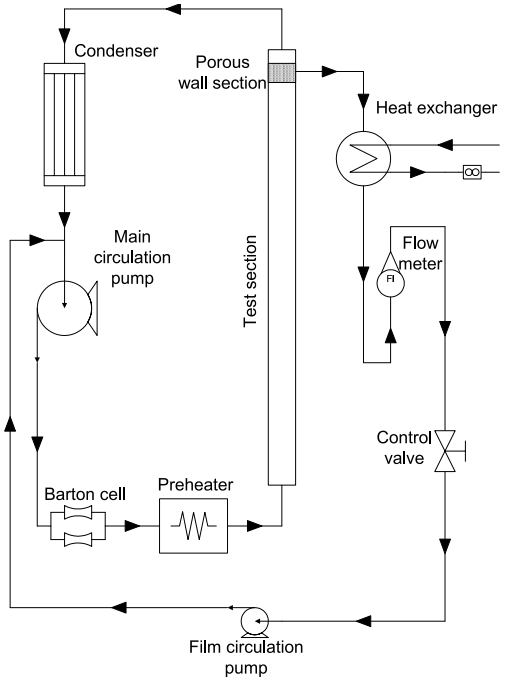

FIGURE 3.1. Working principles of the main loop and the film extraction loop.

3.2. Present Experimental Setup

The working principle of the main loop and the film measurement system is shown in Fig. 3.1. Before the test-section, the water passed through a 150 kW preheater to achieve the desired inlet temperature. The test-sections were manufactured from 3.65 m long stainless steel pipes with 14 mm inner diameter and were heated by an electric current (DC) in the steel. The power was calculated as the product of this current and the voltage over the test-section and the power distribution was imposed by letting the outer diameter of the pipe vary (thereby varying the electrical resistance).

The power distributions that were studied in the present work are shown in Fig. 3.2. (The power distributions shown are the actual power distributions obtained by measuring the local electrical resistance of the test-sections). These four distributions – the uniform, inlet peaked, middle peaked and outlet peaked – were chosen to be able to study the well documented effect of decreasing dryout power when the power peak moves towards the exit and since a large amount of dryout data are available for these distributions.

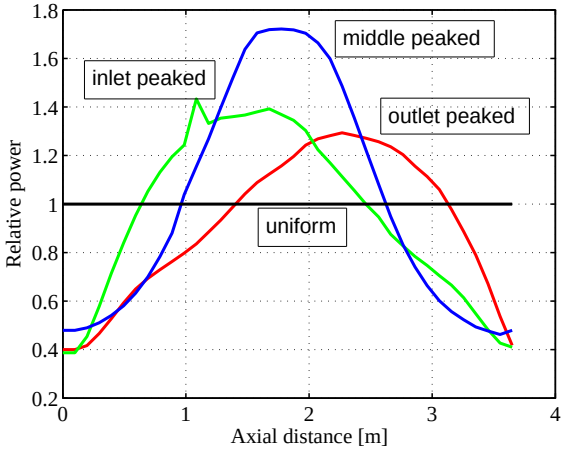

FIGURE 3.2. The four axial power distributions used in the experiments. The spike in the inlet peaked distribution is a manufacturing fault.

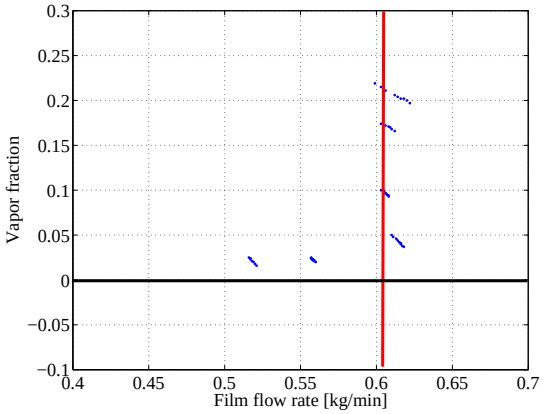

FIGURE 3.3. Example of suction curve from the experiments. The film flow rate is determined from the intersection of the vertical part of the curve with the horizontal axis.

The water was then condensed before it passed through the main circulation pump and the flow measurement system, which consisted of four 1000 mm long pipes with various diameters. The flow rate measurements were based on measuring the pressure drop over one of these pipes with a Barton cell.

To this was added the film extraction loop with a heat exchanger, flow meter and a second circulation pump. The purpose of the heat exchanger was to condense the extracted sample before it entered the flow meter. The vapor content could then be calculated by monitoring the temperatures and flow rates at the primary and secondary sides of the heat exchanger. These calculations, which were carried out automatically by a LABVIEW software during the measurements, are described in detail in Paper 3.

The results were analyzed graphically by plotting the extracted liquid flow rate against the vapor fraction in the sample to obtain an L-shaped curve as shown in Fig. 3.3. The film flow rate could be read off as the intersection of the vertical part of the curve with the horizontal axis. (For details about the analysis of the extraction curves and more examples, see Paper 1 and Paper 3).

Figs. 3.4 and 3.5 show photographs of the film extraction device and the sinter metal section that was used in the experiments. Note the small distance between the power clamp to the right in Fig. 3.4 and the extraction point. It is important to have this distance as small as possible to prevent redeposition of drops before the measurement point.

The heat exchanger was placed as close as possible to the extraction point and was well insulated to prevent heat losses in the connection pipe. Several thermocouples were used to measure the various temperatures at the primary and secondary sides. This redundancy in the temperature measurements made it easier to estimate the accuracy (Section 3.4).

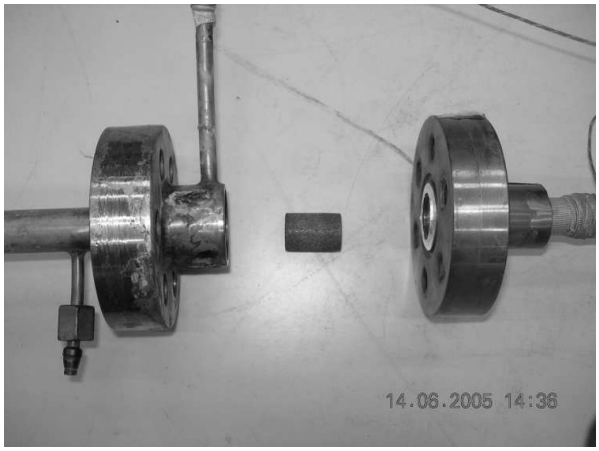

FIGURE 3.4. Side view of dismounted film extraction device.

FIGURE 3.5. The porous sinter metal part mounted in the film extraction device.

3.3. Measurement Procedure

For each experiment the first step was to establish steady-state in the main loop at the desired conditions. The sample flow rate through the porous wall was then adjusted to a low value (compared to the expected film flow rate). After a couple of minutes a steady-state had developed in the main loop and the heat exchanger in the film extraction loop. (The LABVIEW software used had functions to help the operators maintain the steady-state during the measurements). All monitored parameters of the system were then saved, the sample flow rate was increased and a new steady-state was allowed establish itself. This continued until as much as possible of the expected L-shaped curve was obtained, which could usually be accomplished within half an hour.

The use of stainless steel implied that the test-section could not withstand post-dryout conditions (other options were considered but ruled out for practical reasons). Hence all experiments had to be performed with some margin to the dryout condition. The procedure used was to start each series of measurements by finding the dryout power at the corresponding flow rate. The steam quality was then reduced by approximately 3% and the film flow measurements started from that lower power. A second series of measurements was also carried out at approximately 10% reduced power. (The full matrix of experiments can be found in Paper 3).

For the uniform power distribution the effective axial position of the filter was changed by changing the inlet temperature, thereby moving the onset of boiling without changing the heat flux. This procedure is however not possible for the non-uniform distributions. In these cases the test-sections had to be dismounted, cut and reassembled again.

After this operation the power to the test-section must be adjusted to reproduce the local heat flux (as opposed to the mean). To achieve this, the local heat flux was measured by monitoring the voltage over a short section of the test-section close to the inlet. The local power could then be calculated as the product of this voltage and the current in the test-section.

3.4. Accuracy

The accuracy of the results from measurements is naturally an issue of major importance. The errors that will always be present in any experimental data can be divided in two types – random uncertainties and systematic errors. The random part is caused by the uncertainty of the instrumentation and can relatively easily be analyzed. The systematic errors are due to possible physical effects that were not considered in the analysis of the data. Examples that should be considered are heat losses in the equipment, consequences of waves on the film surface and redepositon of entrained drops before the extraction point.

A thorough analysis of both the random uncertainties and systematic errors can be found in Paper 3. It was concluded that the main source of uncertainties was the flow measurements in the film loop. In the present project a rotameter from KROHNE was used for this purpose. It was calibrated to be accurate within 2% for flow rates between 0.3 and 3.0 kg/min. When the measured film flow rate was small this accuracy was not fully satisfactory and at the end of the project the equipment was complemented with an addition flow meter of turbine type, calibrated for low flow rates. It proved to be more reliable than the rotameter and it is hence recommended to replace the rotameter with a turbine flow meter in future measurements.

It was also concluded in Paper 3 that heat losses in the extraction loop and redeposition of drops were small enough to be neglected. The interpretation of the suction curves, however, sometimes constitutes a significant error source. More examples of exctraction curves can be found in Paper 1 and Paper 3 and it is clear from the figures there that not all the curves had the ideal L-shape shown in Fig. 3.3. Sometimes the deviation could be explained by disturbance waves on the film surface, but in other cases it must be treated as an uncertainty of the measurement equipment. (See Paper 3 for examples and a more detailed discussion of this issue).

Finally it was estimated that measurements with reasonably sharp and readily interpreted suction curves could be considered to be accurate within ± 0.1 kg/min and measurements with distorted suction curves were considered accurate within ± 0.2 kg/min. All error bars shown in this thesis are based on that estimate.

CHAPTER 4

Models and Correlations

Since construction of the first BWRs began a huge amount of dryout measurements have been performed over a very large range of conditions in simple pipes, annuli and various rod bundles. Such measurements clearly show that the dryout power is sensitive to the geometry of the channel. Even small features, such as details of spacer grids, may have a significant impact on the dryout performance, which has led to a continuous optimization of fuel geometry. With this development has followed new dryout models, which account for the changes of fuel geometry. There is also a great interest to improve the accuracy of these models in order to efficiently use the fuel.

Currently, the only models that are used in the operation of reactors are empirical correlations, fitted to the parametric trends from extensive measurement programs (Section 2.2). Such models do not extrapolate well and the interest in more mechanistically based models has always been great, which has lead to the development of film flow analysis.

This chapter first introduces traditional dryout correlation techniques and then proceed with an overview of the current state of film flow analysis.

4.1. Dryout correlations

The results of dryout experiments are typically tabulated as the power when dryout first occurred versus coolant mass flux, inlet coolant temperature and outlet pressure. Provided that other parameters do not vary, such a database can readily be used as a look-up table and give very accurate predictions of the dryout power. A simple dryout correlation can be obtained by fitting an appropriate mathematical expression to the data.

The problems that arise with this simple approach are much connected with the relative power distribution. This is a parameter that is complicated and expensive to vary in a dryout experiment and that cannot be described by a single number, which could act as an entry in a table or parameter to a correlation. The formulation of dryout correlations is thus, to large extent, a search for a method to map the power distribution onto a number that correlates with the dryout power.

There are two major formulations of dryout correlations that have been extensively used. The earliest dryout correlations described the critical heat

flux, q_c'', as a function local steam quality, x. Usually a more or less linear trend was observed so that correlations of the form

$$q_c'' = A - Bx \tag{4.1}$$

could be obtained, where the correlation constants, A and B, are functions of the coolant mass flux and system pressure.

The second approach, which is currently prevailing in various forms, is to correlate the critical steam quality, x_c, against the boiling length, L_B, which is usually defined as the distance from the point where the thermodynamic steam quality is zero to the dryout point. A common form is

$$x_c = \frac{aL_B}{b + L_B} \tag{4.2}$$

where the correlation parameters a and b depend on the mass flux and pressure.

It is easy to show that when the power distribution is uniform the two correlations forms (4.1) and (4.2) are equivalent (Hetsroni 1982). They do, however, respond very differently if the axial power distribution is varied. The boiling length is sensitive to variations of the power profile in the lower, sub-cooled, part of the bundle. A redistribution of power in the boiling part of the bundle, on the other hand, will have no influence on L_B. This effect is quite striking if the boiling length parameter is calculated for the cold patch experiments by Bennett *et al.* (1966) discussed in Section 2.3. Fig. 4.1 shows the experimental dryout power from these experiments and the corresponding boiling length versus the position of the cold patch. Both curves are normalized against a uniform power distribution. As can be seen, L_B is constant except when the cold patch is in the sub-cooled region whereas the dryout power varies by 10%. Obviously a constant L_B can never capture the observed variation regardless of the correlation formulation.

The behavior of heat flux correlations depend on how q_c'' in equation (4.1) is defined. Defining q_c'' to represent the local heat flux at the point where dryout occurs is known as the local conditions hypothesis. This, however, gives a correlation that is highly sensitive to heat flux variations in sharp contrast to experimental evidence (Groeneveld 1975), (Becker *et al.* 1981). The local conditions hypothesis is therefore since long abandoned for BWR applications.

Many alternative definitions of q_c'' have been proposed that would yield a more realistic behavior. This usually involves various averages of the axial heat flux distribution (Yang *et al.* 2006). In this way it is often possible to obtain a formulation that reproduces a particular database within an acceptable error range. The fundamental problem, however, is that usually relatively few power profiles are experimentally tested, while the potential number of power profiles in a realistic reactor core is enormous; there is no reason to believe that *ad hoc* dryout correlations should be able to carry out that extrapolation.

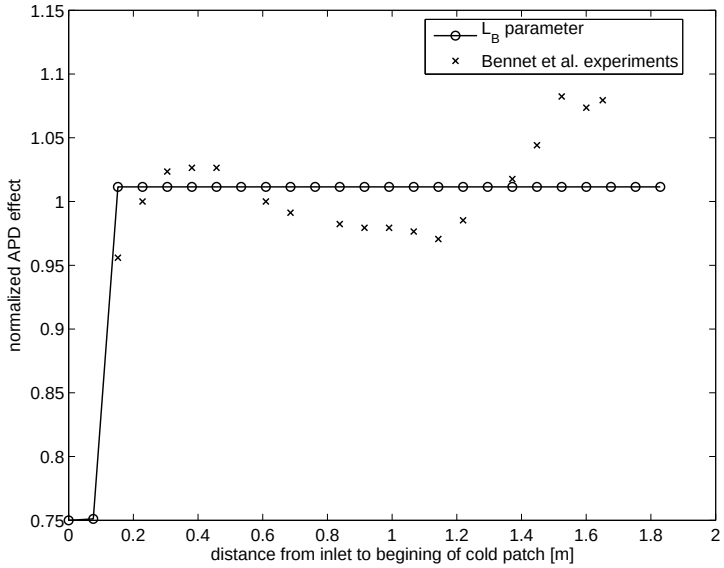

FIGURE 4.1. Relative dryout power and boiling length in experiments by Bennett *et al.* (1966)

4.2. Film-flow models

The axially evolving dynamics between the liquid film and entrained droplets that was discussed in Section 2.3 has to be modeled by a differential equation. In a pipe with a single wetted wall this equation can be formulated by considering a simple mass balance for the film flow rate over a small axial control volume of axial height dz:

$$\frac{dW_f}{dz} = \Pi \left(D - E - \Gamma \right), \tag{4.3}$$

where W_f is the film mass flow rate, Π is the wall perimeter and D, E and Γ denote the deposition, entrainment and evaporation rates, respectively. In order to close this model the three source terms on the right hand side need to be modeled and the equation has to be equipped with an appropriate boundary condition. The evaporation rate is easily modeled by assuming thermal equilibrium, i.e. that all heat that enters the coolant is immediately used to evaporate the film. This gives:

$$\Gamma = \frac{q''}{h_{fg}}, \tag{4.4}$$

where q'' is the wall heat flux and h_{fg} is the latent heat of the coolant.

The remaining terms are the main challenges of film-flow analysis and naturally subject to continuous development; the sections below are an attempt to summarize the current state-of-the-art.

4.2.1. *Deposition models*

The current knowledge about the deposition process was outlined in Section 2.1.1. It was concluded that, even though the roles of various mechanisms are still unclear, it is a common assumption that deposition of droplets is driven by turbulent dispersion. Accordingly, the deposition rate is commonly modeled as proportional to the effective density of droplets in the vapor core, C:

$$D = k_D C, \tag{4.5}$$

where the deposition coefficient, k_D, is correlated against measurements. The effective droplet concentration is usually defined as

$$C = \frac{W_d}{\frac{W_d}{\rho_l} + \frac{W_g}{\rho_g}}, \tag{4.6}$$

where W_d is the mass flow rate of droplets and ρ_l and ρ_g are the liquid and gas densities, respectively. It should be noted that eq. (4.6) assumes that droplets and vapor move with the same average velocity. This assumption is not realistic but eq. (4.6) may still be a useful definition. It is then important to use the same definition of C when the correlation is applied, e.g. in a three-field model of annular flow (Chapter 5), even though a amore accurate model of the droplet density may then be available.

A large number of correlations for k_D have been proposed, e.g. (Sugawara 1990), (de Bertodano & Assad 1998), (Utsuno & Kaminaga 1998), (Hewitt & Govan 1990). These correlations can all be put on the following non-dimensional form:

$$\frac{k_D}{k_D^*} = \text{function}\left(\text{Re}_g, \frac{C}{\rho_g}, \text{Sc}\right), \tag{4.7}$$

where Re_g is the gas Reynolds number and Sc is the Schmidt number. k_D^* is the superficial gas velocity except in the case of the correlation by Hewitt & Govan (1990) who used

$$k_D^* = \sqrt{\frac{\sigma}{\rho_g d}}, \tag{4.8}$$

where d is the pipe diameter and σ denotes the surface tension. This correlation has later been modified and improved by Okawa *et al.* (2003) and Okawa & Kataoka (2005).

The choice of the scale (4.8) is interesting, since it depends on the surface tension, which is related to the droplet size but not to the the gas velocity. It has the advantage to follow the observed difference in deposition rates between high pressure steam-water flows and experiments at atmospheric conditions (Section 2.1.1).

It was noted in Section 2.1.1 that the deposition rate seems to be almost independent on the gas velocity. Accordingly, the correlations that are built on the deposition scale (4.8) do not include any dependency on the Reynolds number whereas the correlations that are built on the gas velocity all have negative dependency on the Reynolds number.

Finally it can be noted that deposition correlations are usually developed and verified based on measurements in round pipes, whereas they are typically applied to rod bundles. It is commonly assumed that the transition can be made by replacing any occurrence of the pipe diameter in the correlation with the hydraulic diameter of e.g. a subchannel (Chapter 5). There is, however, not much direct verification of this approach.

4.2.2. *Entrainment models*

The entrainment phenomenon was discussed in Section 2.1.2. It was concluded that several mechanisms are possible all of which are only qualitatively understood. It then should not come a surprise that a large number of correlations are available. There is also a large disparity of correlation forms, which are often dimensional, adding to the sense of uncertainty as to the validity of these expressions. A few examples of commonly used and relatively recent correlations that also appear in Papers 2–5 will be discussed below.

The lack of direct measurements of entrainment implies that all existing experimental data relies on the use of a deposition correlation , as was discussed in Section 2.1.2. This means that entrainment correlations should not be discussed separately from the corresponding deposition correlation. All correlations discussed in this section, however, rely on closely related variants of the deposition correlation published by Hewitt & Govan (1990).

Okawa et al. have, in a series of papers (Okawa *et al.* 2003), (Okawa *et al.* 2004), (Okawa & Kataoka 2005), hypothesized that the rate of shear induced entrainment, E, depends on the ratio of the shear stress acting on the film surface to the surface tension. It was described by the following non-dimensional group

$$\pi_E = \frac{f_i \rho_g J_g^2}{\sigma/\delta}, \tag{4.9}$$

where ρ_g is the gas density, J_g the gas superficial velocity and δ represents the average film thickness. f_i is the wall friction factor that was modeled according to Wallis (1969) as

$$f_i = 0.005 \left(1 + 300\frac{\delta}{d}\right). \tag{4.10}$$

The film thickness was calculated from the following simple force balance

$$f_i \rho_g J_g^2 = f_w \rho_l \left(\frac{d}{4\delta} J_f\right)^2, \tag{4.11}$$

where J_f is the film superficial velocity and f_w is the wall friction factor that may be set equal to 0.005 for simplicity. Eq. (4.11) relies on several assumption, which are discussed in Okawa & Kataoka (2005) (thin film, low liquid volume fraction, neglect of gravity, among other).

The following correlation form was then assumed

$$E = k_E \rho_l \pi_E^n, \tag{4.12}$$

where the exponent n and the coefficient k_E where correlated as functions of π_E. The parameter k_E has the dimension of a velocity, which is a weakness of this formulation since, by similarity analysis, k_E must then depend on some more fundamental dimensional parameter. This dependency is missing from the correlation and was not discussed by the inventors.

Another correlation that is strictly non-dimensional was proposed by Hewitt & Govan (1990). It can be formulated as:

$$\frac{E}{G_g} = 5.75 \cdot 10^{-5} \left(\left(G_f - G_{f,\mathrm{crit}}\right)^2 \frac{d_h \rho_l}{\sigma \rho_g^2} \right)^{0.316}, \tag{4.13}$$

where G_f and G_g are the mass fluxes of film and vapor respectively. $G_{f,\mathrm{crit}}$ represents the lowest film flow where entrainment occurs and was given by a separate correlation.

A common issue of the correlations (4.12) and (4.13) is that the formulations are applicable only to a channel with a single liquid film. (Chapter 5 discusses applications with multiple liquid films). This issue can be remedied by careful reformulation of the correlations, which also brings some light on the form of correlation (4.13), which was not discussed much by the inventors.

The film mass flux, G_f, which is defined based on the pipe cross-section area cannot be used if several independent films are present. A generalization may be constructed by assuming that the film flow rate per unit wall perimeter is the parameter that is locally relevant and using the relation

$$G_f = \frac{4}{d_h} \frac{W_f}{\Pi}. \tag{4.14}$$

By substituting (4.14) into (4.13) and rearranging one obtains

$$\frac{E}{G_g} = 5.75 \cdot 10^{-5} \cdot \mathrm{We}_f^{0.316} \cdot \left(\frac{\rho_l}{\rho_g} \right)^{0.632} \tag{4.15}$$

where We_f is the follwing modified film Weber number

$$\mathrm{We}_f = \left(\frac{W_f - W_{f,\mathrm{crit}}}{\Pi} \right)^2 \left(\frac{16}{\rho_l \sigma d_h} \right). \tag{4.16}$$

This form of the correlation (4.13) is locally valid. The appearance of the Weber number also adds some physical credibility to the formulation.

In case of correlations of the form (4.12) the definition (4.9) is local enough while equations (4.10) and (4.11) need consideration. The latter contains the superficial film velocity, J_f, which can be replaced by $J_f = G_f/\rho_l$ and equation (4.14). Equation (4.10) appears to be on local form, but it is questionable whether different walls in the same subchannel can have different interfacial friction factors. Since the shear stress tends to distribute evenly on the channel walls when the flow is turbulent it may be more accurate to use a constant friction factor based on the volume occupied by the liquid film:

$$f_i = 0.005\left(1 + 75\frac{\sum_k \Pi^k \delta^k}{A}\right), \tag{4.17}$$

where k enumerates walls and A is the cross-section area of the subchannel. Note that equation (4.17) reduces to (4.10) if only a single film is present.

4.2.3. *Boundary condition*

Equation (4.3) is valid only for the annular flow regime. A natural boundary condition is therefore to specify the film flow rate at the onset of annular flow. This boundary condition is probably the most uncertain part of phenomenological dryout modeling, primarily because very few film flow measurements, if any, in these region exist (Paper 3). On the other hand the boundary condition is not necessarily very important; if the channel is long enough any influence of the dryout condition will have disappeared before the dryout point. BWR fuel bundles (heated length around 3.8 m) seem to be in a region where the influence of the boundary condition is small but not entirely negligible (Paper 4).

A common assumption is that deposition and entrainment are in equilibrium at the onset of annular flow. This assumption was successfully used by Okawa *et al.* (2003), who used a correlation by Wallis (1969) for the transition to annular flow and calculated the film flow rate by setting the deposition and entrainment correlations equal at that point.

Hewitt & Govan (1990) mention the assumption of 99% of the liquid to be entrained as drops at a quality of 0.1, but also that their results were insensitive to this assumption. Since this boundary condition would not reproduced the data presented here, the boundary condition given by Okawa *et al.* (2003) was used instead (Paper 3).

4.2.4. *Models of the critical film thickness*

The possibility of a critical film thickness was discussed in Section 2.1.3. Even though it is unclear whether this phenomenon has any significant influence models of the critical film thickness have been included in several codes that perform film flow analysis (Hoyer 1998), (Chun *et al.* 2003).

Okawa *et al.* (2003) used a critical film model developed by Ueda & Isayama (1981) but showed in a parameter study that this model did not have a significant influence on the predicted dryout power.

The issue has a certain significance since the critical film thickness is often modeled as dependent on the local heat flux. If such a model is added with incorrect sensitivity it may interfere with the power distribution, creating erroneous trends when extrapolating.

CHAPTER 5

Subchannel models

Most nuclear reactors use fuel assemblies with fuel rods arranged in a more or less regular square lattice. Approximating this as a pipe with e.g. preserved cross-section area and hydraulic diameter is sufficient for some thermal-hydraulic applications but for accurate dryout predictions it is usually not. The reason is that the power of the individual fuel rods in an assembly may vary significantly for a number of reasons, such as inserted control rods, use of various enrichments and burnable absorbers among other. Modern, highly optimized, fuel assemblies also contain large water rods, part-length rods and other irregular features. Fig. 5.1 illustrates a realistic power profile and fuel geometry. It should be clear that, in general, a fuel assembly cannot be modeled as one-dimensional channel but must be viewed as a three-dimensional structure.

As was briefly discussed in Chapter 4 dryout correlations may account for these features by the use of various corrections. Such models, however, must be carefully tuned against a large database of accurate dryout experiments and, even then, the ability of such corrections to interpolate the experimental data correctly is questionable.

These issues call for models of two-phase flows on a finer level than the fuel assembly. On the other hand, on the microscopic level the laws of two-phase flows are not well understood. A commonly used compromise is to consider the fuel bundle as a set of interconnected subchannels, defined as the space in between four fuel rods (Fig. 5.2). The subchannel approximation provides a coarse but three-dimensional description of the flow pattern but at the same time the individual subchannels resemble simple pipes for which much experimental data and phenomenological models are available.

Subchannel modeling is currently more common for PWR than for BWR applications, but the latter are quickly developing and begin to be used as standard engineering tools. Because of the more complex geometry of BWR fuels the concept of a subchannel has to be extended to include subchannels defined by e.g. two fuel rods and an unheated wall. Such non-symmetric subchannels are indicated in Fig. 5.2 as 'wall' and 'corner'. It is briefly discussed in Paper 4 that the accuracy of currently available subchannel models for BWR fuel is not satisfactory in such subchannels.

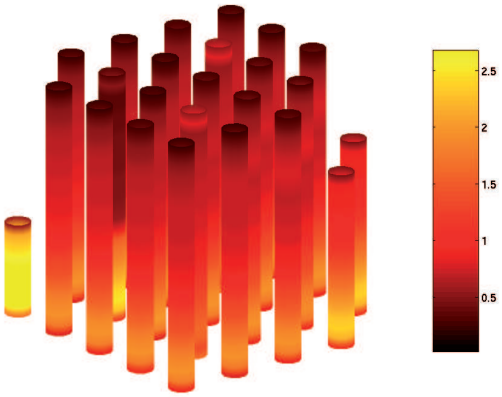

FIGURE 5.1. Three dimensional power distribution. Part-length fuel rods are visible.

It is not obvious how dryout models are best included in subchannel codes. Standard methodology for PWR involves the application of empirical DNB correlations on the subchannel level in a fuel bundle. This approach has been suggested also for dryout models applicable to BWR fuel (Kolev 2007). Such a model, however, would rely on a dryout correlation for the influence of the axial power distribution, while using the subchannel model for lateral effects. This seems unsatisfactory considering the poor treatment of axial effects by all known dryout correlations (Section 4.1).

This chapter provides an overview of two different approaches to subchannel modeling of two-phase flows — the two-field and the three-field concepts — and introduces a, partly novel, hybrid between the two. The present discussion is concerned with the annular flow regime and the integration of dryout models in the subchannel approximation. Subchannel codes in general have many other applications, but a discussion of these would lead beyond the scope of this text.

5.1. Two-field subchannel codes

Many subchannel codes include a model of the annular flow regime but not a film model and are hence adequately described as two-phase, two-field. One example of such a code is VIPRE-01 (Stewart *et al.* 1989) that was used for calculations presented in Papers 4 and 5.

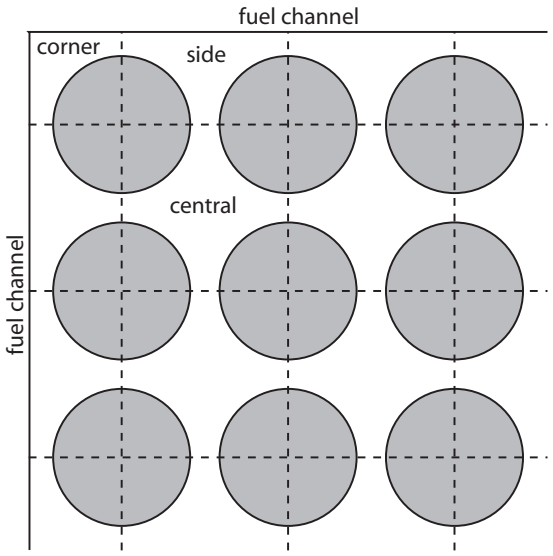

FIGURE 5.2. Typical subchannel decomposition in part of a BWR fuel bundle. Three distinct subchannel geometries arise: central, side and corner.

Despite a certain complexity, two-field subchannel codes execute quickly on modern computers and are usually numerically robust. A solution for a typical BWR fuel assembly can often be produced in a few seconds on a standard office computer. This may be a considerable advantage over more complex models as a nuclear reactor may contain a thousand fuel assemblies and repeated and sometimes fast analysis may be necessary.

5.1.1. *Axial conservation equations*

The main assumption of the subchannel approximation is that flow can be considered to be purely in the axial direction in most of the subchannel. The small lateral flows in between subchannels are called crossflows and are treated as source terms in the equations that describe the axial flow. These equations can be derived by considering a control volume in the form of thin slab of height dz through the subchannel. For simplicity the equations are given here for steady-state conditions only. Time dependent formulations are given by Lahey & Moody (1993).

Conservation of mass in the control volume gives

$$\frac{dW_{m,i}}{dz} = \sum_j w'_{ij}, \tag{5.1}$$

where $W_{m,i}$ is the mixture mass flow rate in subchannel i and w'_{ij} is the crossflow from subchannel j into subchannel i per unit axial length. Conservation of energy over the same control volume leads to the following equation:

$$\frac{d}{dz}\left(W_{m,i}h_{m,i}\right) = \sum_j w'_{ij}h_{CF,ij} + \Pi q'' + \sum_j S_{ij}q''_{TM} \tag{5.2}$$

where $h_{m,i}$ is the mixture enthalpy of subchannel i, h_{CF} is the enthalpy of the crossflow, Π and q'' denote the wall perimeter and heat flux respectively and q''_{TM} is the heat transfer rate due to turbulent mixing (Section 5.1.2). S_{ij} denotes the gap width between subchannels i and j. Finally, conservation of axial momentum gives

$$\frac{1}{A}\frac{d}{dz}\frac{W_{m,i}^2}{A\rho_{\text{mom}}} + \sum_j \left(M_{CF,ij} + M_{TM.ij}\right) = \frac{dP}{dz} - \rho_m g - \frac{f_i}{d_h}\frac{W_{m,i}^2}{2A^2\rho_l}\Phi_{lo}^2 - ..., \tag{5.3}$$

where f_i and Φ_{lo}^2 are a flow friction factor and two-phase multiplier, respectively, P is pressure, A is the subchannel cross-section area, g is the gravitational acceleration and $M_{CF,ij}$ and $M_{TM,ij}$ account for momentum transfer by crossflows and turbulent mixing, respectively. The three dots at the end of equation (5.3) indicate that other pressure losses may be present, e.g. from spacer grids.

The momentum density is defined as (Lahey & Moody 1993)

$$\rho_{\text{mom}} \equiv \left[\frac{(1-x)^2}{\rho_l\left(1-\alpha\right)} + \frac{x^2}{\rho_g\alpha}\right]^{-1}. \tag{5.4}$$

Here α is the volume fraction of vapor, commonly known as the void fraction, and x is the steam quality, which, assuming thermal equilibrium, is given by

$$x = \frac{h_m - h_{l,\text{sat}}}{h_{fg}}, \tag{5.5}$$

where $h_{l,\text{sat}}$ is the liquid saturation enthalpy and h_{fg} is the latent heat.

Expression (5.4) does not correspond to any measurable density; it is just a definition that accounts for the fact that the phases move at different velocities. A specific model of this phase slip is needed in order to have a closed system of equations. It is usually given as a semi empirical relation between the void fraction and steam quality, most commonly by some version of the drift flux model (Lahey & Moody 1993).

Equations (5.1)–(5.3) are the main differential equations that need to be descretized and solved for each subchannel. In addition all crossflow source terms need to be modeled. Since these terms will, in general, depend on properties from two neighboring subchannels the equations for all subchannels will couple and form one large system of equations.

5.1.2. *Crossflow modeling*

The modeling of crossflows is an essential but uncertain part of subchannel analysis since many complex phenomena are involved. The crossflows are typically divided into flow diversions that are due to lateral pressure gradients, turbulent mixing due to stochastic motions and void drift effects, which refer to the tendency of the gas phase to drift towards high velocity regions. None of them are easy to model and the understanding of especially the void drift is far from complete. The subject is only briefly outlined here to illustrate the type of reasoning that is involved.

The crossflow velocity, j_{CF}, may be related to the lateral pressure difference, Δp_{gap}, by a friction factor approach

$$\Delta p_{gap} = -\frac{1}{2} K_G \frac{\rho_{CF} j_{CF}}{S}, \tag{5.6}$$

where K_G is a constant describing the resistance to crossflows, ρ_{CF} is the mixture density of the crossflow and S denotes the gap width. The enthalpy of the crossflow is commonly determined from the donor subchannel, i.e. the subchannel at the upstream end of the crossflow. There is, however, some experimental data that indicate that the crossflow enthalpy is larger than that of the donor channel (Lahey & Moody 1993), pp 178.

Turbulent mixing is commonly viewed as a stochastic exchange of 'globs' of fluid of equal volume between two subchannels (Fig. 5.3). In a single-phase flow, where the density is constant, there would be no mass exchange but a possible exchange of enthalpy between the two subchannels. This turbulent, oscillating volume flux may be expressed in terms of the eddy diffusivity ϵ as

$$j_{\mathrm{TM}} = \frac{\epsilon}{l_{ij}}, \tag{5.7}$$

where l_{ij} denotes the distance between subchannel centroids. The eddy diffusivity may by modeled according to the mixing length theory (Lahey & Moody 1993).

It follows that the equivalent heat flux due to turbulent mixing may be expressed as:

$$q''_{TM,ij} = \frac{\epsilon}{l_{ij}} \left[\left(\rho_l h_l \left(1 - \alpha_i \right) + \rho_g h_g \alpha_i \right) - \left(\rho_l h_l \left(1 - \alpha_j \right) + \rho_g h_g \alpha_j \right) \right], \tag{5.8}$$

and the momentum transfer becomes

$$M_{TM,ij} = \frac{S_{ij} \epsilon}{l_{ij}} \left(\frac{W_i}{A_i} - \frac{W_j}{A_j} \right). \tag{5.9}$$

In a two-phase flow there may be a difference in mixture density between the subchannels. In that case the turbulent mixing will induce a net mass transfer:

$$w'_{\mathrm{TM},ij} = \frac{S_{ij} \epsilon}{l_{ij}} \left(\rho_i - \rho_j \right), \tag{5.10}$$

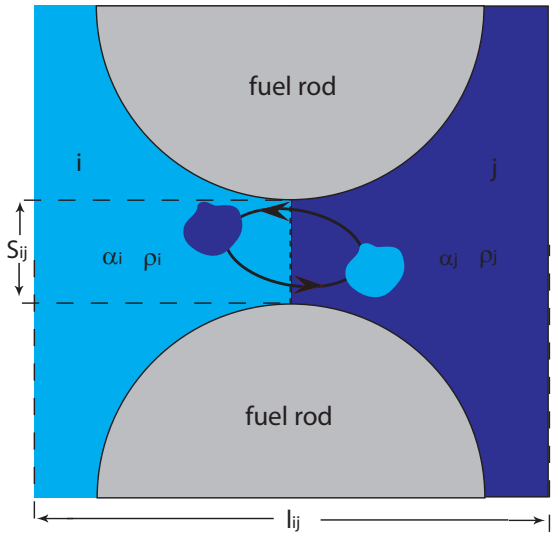

FIGURE 5.3. Idealized view of turbulent mixing in the gap between two subchannels. Fluid 'globs' of equal volume are exchanged; a density gradient between the subchannels will cause a net mass flow down the gradient.

where S_{ij} is the subchannel gap width. This blurs the distinction between turbulent mixing and flow diversion crossflows. (This issue can be avoided by postulating an exchange of equal masses, rather than volumes, but that seems rather difficult to motivate from a mechanistic point of view).

The turbulent mixing model will work in the direction of a uniform void distribution in a fuel bundle. This is not consistent with available experimental data which shows that the gas phase tends to accumulate in open areas with high velocity. This phenomenon is called void drift but is not completely understood. If models of void drift are included in subchannel codes they are therefore usually more or less *ad hoc*.

The above examples illustrate the complexity of crossflow modeling in two-phase flows and the phenomenological approach that is used. Naturally, such models are carefully optimized and validated with experimental data, which may give accurate and reliable results. However, the phenomenological approach indicates that they should not be trusted for conditions for which they were not developed and verified.

5.2. Three field subchannel codes

By introducing a separate mass equations for the liquid film and droplets a three-field, two-phase model of the annular flow regime is obtained. The three

mass equations may be formally written as

$$\frac{dW_{f,i}^k}{dz} = \Pi_i^k \left(D_i - E_i^k - \Gamma_i^k\right) + \sum_j w'_{f,ij} \tag{5.11}$$

$$\frac{dW_{d,i}}{dz} = \sum_k \Pi_i^k \left(-D_i + E_i^k\right) + \sum_j w'_{d,ij} \tag{5.12}$$

$$\frac{dW_{g,i}}{dz} = \sum_k \Pi_i^k \Gamma_i^k + \sum_j w'_{g,ij}, \tag{5.13}$$

where subscript i enumerates subchannels and superscript, k, enumerates wetted walls within a subchannel and f, d and g denote film, droplets and gas fields, respectively. $w'_{f,ij}$ represents the crossflow of film from subchannel j into subchannel i and correspondingly for the drop and gas fields.

In general there would be axial conservation equations also for the momentum and energy for each field, i.e. nine equations for each subchannel. This is the case in e.g. the COBRA-TF code (Thurgood *et al.* 1983). However, some of these equations may be combined; for example, the MONA code (Nordsveen *et al.* 2003) combines the momentum equations of the droplet and gas fields and the energy equations of the film and droplet fields, respectively but can still be considered as a three-field code since there are separate mass balance equations for gas, droplets and film.

Separate momentum equations for the film and the core of the annular flow pattern allows explicit modeling of the phase slip by an interfacial friction factor that replaces the void model and two-phase multiplier that are necessary in two-field models (Section 5.1). However, the main advantage of a three-field model is that it allows the dryout phenomenon to be treated by film flow analysis as outlined in Chapter 4. This offers a realistic method to simulate effects of complex three dimensional power distributions in rod bundle geometry.

The modeling of three-field crossflows is at least as complex as the two-field case. In principle the same models that were outlined in Section 5.1.2 can be used but liquid and gas crossflow have to be explicitly separated since they enter equations (5.11)–(5.13) as separate source terms. In principle a three-field code would also need to model the crossflows of film and droplets separately. This issue is discussed in Section 5.3.

5.3. MEFISTO hybrid approach

Paper 4 and Paper 5 develop an approach to film-flow subchannel modeling that essentially relies on a two-field subchannel code to calculate the distribution of flow and enthalpy in the bundle and applies a film-model as post-process that splits the liquid phase into droplets and liquid film. Another feature that is usually not included in three-field codes is that MEFISTO uses separate fields for the films on each of the subchannel walls. This capability is necessary to

model subchannels if there are significant differences in heat-flux among the walls, an extreme example being one or more unheated walls. (Formally the MEFISTO code thus handles an arbitrary number of fields).

The idea behind this approach was to combine the film-modeling capabilities of three-field codes with the fast and robust execution of two-field codes. The latter is an important feature not only because of the applicability of the final code to tasks where run-time is essential; it also allows extensive testing and complex optimization algorithms that would be practically unfeasible to apply to a full three-field code. High axial resolution may also be a crucial part of an accurate dryout model, but could drive run-times of three-field codes to unpractical levels.

The MEFISTO code achieves speed-up by an order of magnitude (Paper 4) compared to full three-field codes by decoupling the film-flow analysis from the calculation of crossflows as described below.

The two-field driver code is first executed to obtain the distribution of gas and liquid. From this solution the net crossflow of gas into subchannel i can be calculated as

$$\sum_j w'_{g,ij} = \frac{dW_{g,i}}{dz} - \sum_k \Pi_i^k \Gamma_i^k. \tag{5.14}$$

It follows by the conservation of mass that the net crossflow of liquid into subchannel i is

$$\sum_j \left(w'_{d,ij} + w'_{f,ij}\right) = \frac{dW_i}{dz} - \sum_j w'_{g,ij} = \frac{dW_i}{dz} - \frac{dW_{g,i}}{dz} + \sum_k \Pi_i^k \Gamma_i^k, \tag{5.15}$$

where $W_i \equiv W_{f,i} + W_{d,i} + W_{g,i}$ is the total mass flow in subchannel i. These equations constitute the first assumption introduced in the MEFISTO code, which may be summarized as: the two-field driver code accurately calculates the flow and enthalpy distribution. The validity of this assumption is discussed in Paper 4.

The second assumption concerns the splitting of the total liquid crossflow, given by equation (5.15), into the droplet and film crossflows that are needed in equations (5.12) and (5.11). This information cannot be obtained from the two-field driver code. Many more or less plausible hypotheses could be proposed for this parameter. However, a sensitivity study (Paper 4) has shown that it is not a particularly important parameter for typical applications of the code. This fact can be exploited to create a crude but computationally efficient model.

The classical method would be to base any property of the crossflow on information from the donor channel (the subchannel at the upstream end of the crossflow). That is, $w'_{f,ij}$ would be calculated based on information from subchannel j if positive, otherwise on information from subchannel i. This approach has some numerical advantages and seems physically plausible. However, it would couple the film-flow calculations of the subchannels to each other.

By instead calculating $w'_{f,ij}$ based on subchannel i regardless of the direction of the crossflow the subchannels can be analyzed independently of each other, which is a great numerical simplification. It may be done as follows:

$$w'_{f,i} = \chi_i w'_{l,i} \tag{5.16}$$

$$w'_{d,i} = (1-\chi_i)\, w'_{l,i}, \tag{5.17}$$

where $w'_{f,i} = \sum_j w'_{f,ij}$ and analogously for $w'_{d,i}$. $w'_{l,i}$ denotes the total liquid cross-fow and can be calculated from eq. (5.15). There are several options for the crossflow constant χ_i. For example, it can be specified so that the droplet to film ratio in the crossflow is the same as in channel i:

$$\chi_i = \frac{W_{f,i}}{W_{d,i} + W_{f,i}}. \tag{5.18}$$

One could also imagine that entrained droplets easier move between subchannels than the film. In the limit of zero film crossflows this gives:

$$\chi_i = 0. \tag{5.19}$$

Reality may be somewhere in between equations (5.18) and (5.19) but the former has the advantage to eliminate the risk to drive any field to negative values by an inconsistency with the driver code. In any case, it was shown in Paper 4 that impact on the predicted dryout power is insignificant in realistic applications.

It can be noted that the assumption (5.16) implies that the composition of the crossflows $w'_{l,ij}$ and $w'_{l,ji}$ will be different. This is not, strictly speaking, an inconsistency; it may be interpreted as an mass transfer between the droplet and film fields (deposition/entrainment) within the crossflow, even though it has been introduced for numerical, rather than physical reasons.

CHAPTER 6

Summary of Papers

6.1. Summary of included papers

Paper 1

Paper 1 presents the film flow measurement technique that was described in Chapter 3 and the results with uniform power distribution. Based on these measurements it is possible to estimate the critical film thickness (Section 2.1.3).

The measured film thickness was plotted versus steam quality and slightly extrapolated up to the measured critical steam quality. The conclusions were in line with Hewitt *et al.* (1965), i.e. that the critical film thickness is insignificantly small. This does not contradict e.g. Ueda & Isayama (1981) since the conditions were not the same, but for the flow conditions and heat fluxes that are typical for BWR operation it was concluded that the critical film thickness is, for practical purposes, zero.

Paper 2

This paper was published when the measurements with non-uniform power distribution were still ongoing. Therefore only the measurements with uniform and top-peaked power profiles were included.

The paper compares the measured data with deposition and entrainment models by Hewitt & Govan (1990) and Okawa *et al.* (2003). These models are also discussed in Sections 4.2.1 and 4.2.2. The issue of a correct boundary condition at the onset of annular flow was avoided by starting the integration of the film flow model from the most upstream measurement point. In this way the net mass exchange rate (deposition less entrainment) could be studied without any initial bias from the boundary condition.

The entrainment correlation proposed by Okawa *et al.* (2003) included a heat flux dependent term to account for boiling entrainment (Section 4.2.2). Paper 2 concludes that the model agrees better with measurements if this term is omitted. The result suggests that boiling entrainment may not be an important effect at the investigated conditions.

Paper 3

The measurements were described in more detail, all the data was tabulated and conclusions from Paper 1 and Paper 2 were confirmed for the full data set.

The model comparison was extended to include the boundary condition at the onset of annular flow. It was concluded that the boundary condition based on hydrodynamic equilibrium that was proposed by Okawa *et al.* (2003) provided good agreement with the film flow measurements. The same boundary condition could be used also with the deposition/entrainment correlations proposed by Hewitt & Govan (1990) but only if the hydrodynamic equilibrium was based on the model by Okawa *et al.* (2003). This indicates a significant uncertainty in the correlations around the onset of annular flow but that the influence on downstream conditions is rather small.

Paper 4

The MEFISTO code that was introduced in Section 5.3 was described and validated against 1364 dryout measurements from the Westinghouse FRIGG loop (Helmersson *et al.* 2006). The model was calibrated with a subset of 105 measurements points by adjusting constants in the spacer model. When applied to the full database, with three different axial power distribution, the standard deviation in predictions increased from 4.0%, over the calibration subset, to 4.4% over the full database. Moreover the axial and lateral location of dryout was well predicted by the model.

Paper 4 also presents numerous plots of simulated film flow rates, deposition and entrainment rates in subchannel geometry.

The main conclusions are that the MEFISTO code, after calibration with a single power distribution, has a statistical predictive performance that is comparable to fuel-specific empirical dryout correlations and is able to extrapolate to other power distributions. The runtime is around 20 CPU seconds when applied to a quarter bundle with 24 heater rods. This is considerably longer than typical dryout correlations but much less than most three-field subchannel codes.

Paper 4 author contributions

C. Adamsson proposed the decoupled film-flow analysis that is the fundamental idea of the MEFISTO code, formulated the basic equations and implemented the core of the solution algorithm. J.M. Le Corre invented and implemented the automated calibration algorithm and carried out most of the work with the FRIGG validation and the interface to the VIPRE code.

The paper manuscript and implementation of the computer code were joint efforts shared roughly equally between the authors.

Paper 5

This paper is a computational study, performed with the MEFISTO code, focused on the influence of the axial power distribution. Several experiments in various geometries were used as reference: cold patch mesurements by Bennett *et al.* (1966) (Section 2.3), film flow measurements presented in Paper 3 of this thesis, BFBT full-bundle dryout measurements and the Westinghouse FRIGG full-bundle measurements, which were discussed in detail in Paper 4.

The results show that correlations for deposition and entrainment rates often need to be *ad hoc* calibrated to follow the observed trends with pressure and flow rate. The influence of the power distribution, however, appears to be an inherent property of the model; the characterisic features, such as increased dryout power for inlet shifted power distribution, appear for all investigated geometries and flow conditions. The magnitude of this effect is excellently predicted as well, but in some cases calibration of the entrainment correlation to remove an overall bias is needed.

CHAPTER 7

Conclusions and Outlook

This thesis has discussed the dryout phenomenon from an experimental and a theoretical perspective at conditions that are typical for normal operation of a BWR. In particular the influence of the axial power distribution has been studied since this parameter is difficult to handle with traditional methodology.

New measurements , which show the axial development of the film flow rate with various axial power profiles have been presented and shown to be consistent with the established theory of film dryout. Phenomenological models of mass transfer in annular two-phase flow have been evaluated against these measurements. It was concluded that models based on simple hydrodynamic considerations provide reasonable accuracy at the investigated conditions; the possibility of boiling induced entrainment of the film seems to be insignificant.

It has also been shown that the film flow rate tends to zero (within the accuracy of the measurements) when the dryout power is approached. Hence no critical film model should be necessary for the heat flux and flow conditions considered here. Also this conclusion is consistent with earlier measurements at similar conditions.

An novel method to perform film flow analysis on the subchannel level as a post-process to a standard two-field subchannel code has been discussed (the MEFISTO code). It was shown that, with appropriate calibration, this approach predicts the dryout power in rod bundles with an accuracy comparable to empirical correlations. At the same time the computational time was reduced by an order of magnitude compared to standard three-field subchannel codes.

This work may be continued, extended and improved in numerous ways. The need for *ad hoc* calibration shows that the fundamental mass transfer models — the deposition and entrainment correlations — are not always satisfactory. That could be improved only by continued experimental efforts. This may include film flow measurements under various conditions but also more detailed investigations of drop and film dynamics.

Another source of uncertainty are spacer grids, which will always be part of a realistic application. Could spacer models be improved it would greatly improve the reliability of film flow analysis and even be used to improve the design of spacer grids, which would increase the dryout performance significantly.

One piece of valuable information could be added by applying the measurement technique presented in this thesis to pipes with various flow obstacles.

The MEFISTO code is currently limited to stead-state analysis. Dryout analysis during various transients is, however, an important part of safety analysis. For transient conditions there is not much detailed experimental data, but the success of film flow analysis under steady-state conditions indicates that it may be valuable also for transients. The extension of the MEFISTO code to transient conditions is a currently ongoing project.

Acknowledgements

First of all I would like to thank my supervisor Dr. Henryk Anglart for all support during this work.

Without Stellan Hedberg and his technical skills and knowledge the experimental part of this work would not have been possible. He constructed the equipment, repaired it when it broke down and spent many hours in the lab with me during the measurements and error searching. Thanks also to my co-supervisor, Per Person, for sharing his experience, the LABVIEW code for the main loop and for showing a lot of interest in the project.

I'm very thankful to Jean-Marie Le Corre for all the help with the MEFISTO code, fruitful discussions, new insights and efficient preparation of manuscripts. The MEFISTO project would not have been what it is today without all that.

The Swedish Center for Nuclear Technology (SKC) and Westinghouse Electric Company are gratefully acknowledged for their financial support. In particular during the last year I have to thank Stig Andersson for giving me the opportunity and incentive to complete the project.

Finally I would like to thank my colleagues and all the friends I have made at KTH for creating a creative, dynamic, open–minded and exciting working environment. I will miss it.

References

Azzopardi, B. J. 1987 Observations of drop motion in horizontal annular flow. *Chemical Engineering Science* **42** (8), 2059–2062.

Azzopardi, B. J. 1997 Drops in annular two-phase flow. *International Journal of Multiphase Flow* **23** (7), 1–53.

Becker, K. M., Letzter, A., Nylund, O. & Schlin, B. 1981 An experimental study of the effect of the axial heat flux distribution on the dryout conditions in a 3650-mm long annulus. *International Journal of Multiphase Flow* **7** (1), 47–61.

Bennett, A. & Thornton, I. 1961 Data on vertical flow of air-water mixtures in the annular and dispersed flow regions. part i: Preliminary study. *Trans. Inst. Chem. Engrs.* **39**, 101–112.

Bennett, A. W., Hewitt, G. F., Kearsey, H., Keeys, R. & Pulling, D. 1966 Studies of burnout in boiling heat transfer to water in round tubes with non-uniform heating. *Tech. Rep.* R5076. AERE.

de Bertodano, M. L. & Assad, A. 1998 Entrainment Rate of Droplets in the Ripple-Annular Regime for Small Vertical Ducts. *Nuclear Science and Engineering* **129**, 72–80.

Blomstrand, J., Behamin, D., Persson, P. & Hedberg, S. 2000 Loop studies simulating – in annular geometry – the influence of the axial power distribution and the number of spacers in 8x8 bwr assemblies. In *2nd Japanese-European Two-Phase Flow Group Meeting*.

Caraghiaur, D., Adamsson, C. & Anglart, H. 2009 Verification of random walk models to calculate drop deposition in nuclear fuel assemblies. In *The 13th International Topical Meeting on Nuclear Reactor Thermal Hydraulics (NURETH-13)*. Kanazawa City, Ishikawa Prefecture, Japan.

Chun, J., Lee, W., Park, C. & Lee, U. 2003 Development of the critical film thickness correlation for an advanced annular film mechanistic dryout model applicable to MARS code. *Nuclear Engineering and Design* **223** (3), 315–328.

Collier, J. G. & Hewitt, G. F. 1964 Film thickness measurement. *ASME paper 64–WA/HT–41* .

Govan, A. H., Hewitt, G. F. & Ngan, C. F. 1989 Particle motion in a turbulent pipe flow. *International Journal of Multiphase Flow* **15** (3), 471–481.

Groeneveld, D. 1975 The effect of short flux spikes on the dryout power. *Tech. Rep.* AECL–4927. Atomic Energy of Canada Ltd.

Groeneveld, D., Shan, J., Vasic, A., Leung, L., Durmayaz, A., Yang, J., Cheng, S. & Tanase, A. 2007 The 2006 CHF look-up table. *Nuclear Engineering and Design* **237** (15-17), 1909–1922.

Helmersson, S., Limbck, M. & Sderberg, H. 2006 Westinghouse BWR fuel - recent experiences and developments. Salamanca, Spain.

Hetsroni, G., ed. 1982 *Handbook of Multiphase Systems*. Hemisphere Publisher Corporation.

Hewitt, G., Kearsey, H., Lacey, P. & Pulling, D. 1965 Burnout and film flow in the evaporation of water in tubes. *Tech. Rep.* R4864. AERE.

Hewitt, G. & Pulling, D. 1969 Liquid entrainment in adiabatic steam-water flow. *Tech. Rep.* R5374. AERE.

Hewitt, G. F. & Govan, A. H. 1990 Phenomenological modelling of non-equilibrium flows with phase change. *International Journal of Heat and Mass Transfer* **33** (2), 229–242.

Hoyer, N. 1998 Calculation of dryout and post-dryout heat transfer for tube geometry. *International Journal of Multiphase Flow* **24** (2), 319–334.

Kolev, N. I. 2007 Check of the 2005-look up table for prediction of CHF in bundles. *Nuclear Engineering and Design* **237** (9), 978–981.

Lahey, A. R. T. & Moody, F. J. 1993 *The Thermal-hydraulics of a Boiling Water Nuclear Reactor*. American Nuclear Society.

Milashenko, V., Nigmatulin, B., Petukhov, V. & Trubkin, N. 1989 Burnout and distribution of liquid in evaporative channels of various lenghts. *International Journal of Multiphase Flow* **15** (3), 393–401.

Nordsveen, M., Hoyer, N., Anglart, H. & Adamsson, C. 2003 The MONA subchannel analysis code part a: Model description. In *The 10th International Topical Meeting on Nuclear Reactor Thermal Hydraulics (NURETH-10)*.

Okawa, T. & Kataoka, I. 2005 Correlations for the mass transfer rate of droplets in vertical upward annular flow. *International Journal of Heat and Mass Transfer* **48** (23-24), 4766–4778.

Okawa, T., Kotani, A. & Kataoka, I. 2005 Experiments for liquid phase mass transfer rate in annular regime for a small vertical tube. *International Journal of Heat and Mass Transfer* **48** (3-4), 585–598.

Okawa, T., Kotani, A., Kataoka, I. & Naito, M. 2003 Prediction of critical heat flux in annular flow using a film flow model. *Journal of Nuclear Science and Technology* **40** (6), 388.

Okawa, T., Kotani, A., Kataoka, I. & Naitoh, M. 2004 Prediction of the critical heat flux in annular regime in various vertical channels. *Nuclear Engineering and Design* **229** (2-3), 223–236.

Schadel, S. A., Leman, G. W., Binder, J. L. & Hanratty, T. J. 1990 Rates of atomization and deposition in vertical annular flow. *International Journal of Multiphase Flow* **16** (3), 363–374.

Singh, K., Pierre, C., Crago, W. & Moeck, E. 1969 Liquid Film Flow-Rate

in Two-Phase Flow of Steam and Water at 1000Lb/Sq.In.Abs. *AIChE Journal* **15** (1).

Stewart, C., Cuta, J., Montgomery, S., Kelly, J., Basehore, K., George, T. & Rowe, D. 1989 VIPRE-01: a thermal-hydraulic code for reactor cores. *Tech. Rep.* EPRI-NP-2511-CCM-A-Vol.1-Rev.3.

Sugawara, S. 1990 Droplet deposition and entrainment modeling based on the three-fluid model. *Nuclear Engineering and Design* **122** (67).

Thurgood, M., Kelly, J., Guidotti, T. & Kohrt, R. 1983 COBRA/TRAC a Thermal-Hydraulics code for transient analysis of nuclear reactor vessels and primary coolant systems. *Tech. Rep.* NUREG/CR-3046, PNL-4385.

Ueda, T. & Isayama, Y. 1981 Critical heat flux and exit film flow rate in flow boiling system. *International Journal of Heat and Mass Transfer* **24** (7), 1267–1276.

Utsuno, H. & Kaminaga, F. 1998 Prediction of Liquid Film Dryout in Two-Phase Annular-Mist Flow in a Uniformly Heated Narrow Tube. Development of Analytical Method under BWR Conditions. *Journal of Nuclear Science and Technology* **35** (9), 643–653.

Wallis, A. G. B. 1969 *One-dimensional Two-phase Flow*. McGraw-Hill.

Whalley, P., Hewitt, G. F. & Terry, J. 1979 Photographic studies of Two-Phase flow using a parallel light technique. *Tech. Rep.* AERE-R9398.

Würtz, J. 1978 An Experimental and Theoretical Investigation of Annular Steam-Water Flow in Tube and Annuli at 30 to 90 bar. *Tech. Rep.* 372. RisøNational Laboratory.

Yang, J., Groeneveld, D., Leung, L., Cheng, S. & Nakla, M. E. 2006 An experimental and analytical study of the effect of axial power profile on CHF. *Nuclear Engineering and Design* **236** (13), 1384–1395.

Part II

Papers